Modeling the propagation characteristics of chorus using CRRES suprathermal electron fluxes

J. Bortnik, R. M. Thorne

Department of Atmospheric and Oceanic Sciences, University of California,

Los Angeles, California, USA.

N. P. Meredith

British Antarctic Survey, Natural Environment Research Council,

Cambridge, UK.

————

J. Bortnik, and R. M. Thorne, Department of Atmospheric and Oceanic Sciences, University

of California, Los Angeles, CA 90095-1565, USA. (jbortnik@gmail.com, rmt@atmos.ucla.edu)

N. P. Meredith, British Antarctic Survey, Natural Environment Research Council, Madingley

Road, Cambridge, CB3 0ET, UK. (nmer@bas.ac.uk)

Abstract.

In the present paper, phase space density functions of the form $f(v) =$ A_N/v^n are fitted to statistical distributions of suprathermal electron fluxes $(E = 0.213 - 16.5$ keV$)$ from the CRRES satellite, parameterized by L-shell, Magnetic Local Time (MLT), and geomagnetic activity. The fitted distributions are used in conjunction with ray tracing to calculate the Landau damping rates of an ensemble of rays representing whistler-mode chorus waves. The modeled propagation characteristics are compared with observations of chorus wave power from the CRRES satellite, as a function of L-shell, MLT, and magnetic latitude, in various frequency bands, and under various geomagnetic conditions. It is shown that the model results are remarkably consistent with many aspects of the observed wave distributions, including frequency, L-shell, MLT, and latitudinal dependence. In addition, the MLT distribution of wave power becomes characteristically asymmetric during active geomagnetic conditions, with small propagation lengths on the nightside which increase with MLT and maximize on the dayside. This asymmetry is shown to be directly related to the dynamics of the Landau resonant suprathermal electrons which drift around the Earth whilst undergoing scattering and loss due to a variety of plasma waves. Consequently, the suprathermal electrons play an important role in radiation belt dynamics, by controlling the distribution of chorus, which in turn contributes to the acceleration and loss of relativistic electrons in the recovery phase of storms.

1. Introduction

Chorus emissions are naturally-produced electromagnetic waves in the ELF/VLF ($\sim$ 0.1 $-$ 10 kHz) frequency range [e.g. reviews by *Omura et al.*, 1991; *Sazhin and Hayakawa*, 1992], that occur outside the plasmapause predominantly in the dawn sector, and rank among the most intense whistler-mode emissions in the inner magnetosphere [*Koons and Roeder*, 1990; *Meredith et al.*, 2001; *Santolik et al.*, 2004]. They typically occur in a series of short ($\sim$ 0.1 sec), rising tones (though falling and mixed tones are also observed) between $\sim$ 0.2 $-$ 2 kHz/s, in two distinct frequency bands that peak in power near $0.34 f_{ce}$ (lower band) and $0.53 f_{ce}$ (upper band), where f_{ce} is the equatorial gyrofrequency along that field-line [*Burtis and Helliwell*, 1969, 1976], and exhibit a wave power minimum near $0.5 f_{ce}$ [*Tsurutani and Smith*, 1974; *Koons and Roeder*, 1990]. Chorus intensity and occurrence are directly related to geomagnetic activity [*Storey*, 1953; *Tsurutani and Smith*, 1974; *Burtis and Helliwell*, 1976; *Meredith et al.*, 2001; 2003; *Santolik et al.*, 2003, 2004; *Smith et al.*, 1999; 2004; *Spasojevic and Inan*, 2005] and it is generally agreed that the generation mechanism involves cyclotron resonance with eastward-drifting, freshly-injected, unstable electron populations in the $\sim$ 10 $-$ 100 keV range, though the exact generation mechanism remains a topic of intense research [*Helliwell*, 1967, 1995; *Omura et al.*, 1991; *Hattori et al.*, 1991; *Sazhin and Hayakawa*, 1992; *Trakhtengerts*, 1995, 1999; *Nunn et al.*, 1997].

Though chorus has been actively studied for well over 50 years [*Storey*, 1953], it has recently enjoyed a resurgence of interest due to the recognition of its importance in control-ling radiation-belt dynamics [e.g., *Horne and Thorne*, 1998; *Summers et al.*, 1998, 2004; *Horne et al.*, 2003, 2005a,b; *Thorne et al.* 2005a,b; *Spasojevic and Inan*, 2005; *Meredith et*

al., 2002a,b; 2003b; *Miyoshi et al.*, 2003; *Lyons et al.*, 2005; *Smith et al.*, 2004; *Varotsou et al.*, 2005; *Shprits et al.*, 2006] playing a dual role in both the precipitation and acceleration of radiation-belt electrons [*Horne and Thorne*, 2003; *Horne et al.*, 2005b; *Bortnik and Thorne*, 2006]. In the scenario described in the above works, lower energy electrons ($\sim 10 - 100$ keV) generate chorus near the geomagnetic equator through the loss-cone instability and thermal anisotropy, and scatter these electrons into the loss-cone in the process, resulting in decreased fluxes [*Ibid*]. The locally generated waves also interact with higher energy electrons at large pitch-angles, contributing to the acceleration of electrons to relativistic energies [e.g. *Meredith et al.*, 2002a; *Horne and Thorne*, 2003]. Chorus waves then propagate to higher latitudes, where they resonate with relativistic (MeV) electrons leading to both microburst precipitation, and further acceleration of trapped relativistic electrons [*Horne and Thorne*, 2003; *Horne et al.*, 2005b]. Chorus thus plays a mediating role, transferring energy from the abundant lower energy electron population to the smaller population of higher energy electrons [e.g., *Thorne et al.*, 2005b; *Horne et al.*, 2006]. In order to properly quantify this mediation process, it is important to understand the propagation characteristics of chorus, its wave normal evolution, damping, and resultant distribution of power with respect to latitude, L-shell, and magnetic local time (MLT).

Previous studies have shown that chorus typically occurs between $3 < L < 9$, with a peak at $6 < L < 8$ [*Tsurutani and Smith*, 1974; *Burtis and Helliwell*, 1976; *Meredith et al.*, 2001], in the dawn and afternoon sectors, moving to higher L-shells and/or latitudes when moving towards the day side [*Burtis and Helliwell*, 1976; *Meredith et al.*, 2001]. Wave normal studies show that near the geomagnetic equator, the **k**-vector is

73 predominantly field-aligned [*Burton and Holzer*, 1974; *Goldstein and Tsurutani*, 1984]

74 in agreement with theoretical predictions [*Kennel and Thorne*, 1967] but becomes pro-

75 gressively more oblique as it propagates away from the equatorial generation region in

76 a non-ducted mode [*Thorne and Kennel*, 1967; *Burton and Holzer*, 1974; *Goldstein and*

77 *Tsurutani*, 1984]. However, recent observations of chorus, particularly at off-equatorial

78 positions, indicate that generation may have occurred at much higher wave normal angles

79 [*Lauben et al.*, 2002; *Chum and Santolik*, 2005; *Santolik et al.*, 2006]. In both cases, prop-

80 agation is found to be away from the equatorial region [*LeDocq et al.*, 1998; *Lauben et al.*,

81 2002; *Santolik et al.*, 2004, 2005], with very few exceptions where weak magnetospheric

82 reflections have been observed [*Maeda and Smith*, 1981; *Parrot et al.*, 2003, 2004]. There

83 is strong support for the fact that propagation is predominantly nonducted [e.g., *Burton*

84 *and Holzer*, 1974; *Goldstein and Tsurutani*, 1984; *Lauben et al.*, 2002; *Chum et al.*, 2005]

85 and apparently limited by Landau damping [*Bortnik et al.*, 2006] to propagation ranges

86 of $10° − 20°$ in latitude [*Burtis and Helliwell*, 1976; *Meredith et al.*, 2001].

87   The relation of chorus morphology to the storm-time injection and dispersive (eastward)

88 azimuthal drift of energetic electrons has been well-noted by past workers [*Anderson and*

89 *Maeda*, 1977; *Collier and Hughes*, 2004a,b; *Smith et al.*, 2004; *Abel et al.*, 2006; *Lubchich*

90 *et al.*, 2006], where the electrons were treated as the source of the chorus waves. In

91 the present work, we neglect all aspects of the wave generation process, and consider

92 only the (linear) Landau damping of the chorus waves as they propagate in an unducted

93 mode away from their source region. Specifically, we examine the effects of suprathermal

94 electron fluxes upon chorus propagation characteristics using a combination of measured

95 fluxes, ray tracing, and comparison to wave data. In Section 2, statistical averages of

96 suprathermal fluxes from the CRRES satellite are presented, parameterized by MLT, *L*-

97 shell, and geomagnetic activity (Sec. 2.1), and analytical phase space density functions

98 are fitted to these measurements (Sec. 2.2). In Section 3 the ray tracing and Landau

99 damping methodology is presented using a single ray (Sec. 3.1), and the results of ray

100 tracing a large distribution of rays are shown (Sec. 3.2). The ray tracing results are

101 compared to chorus wave measurements made on the CRRES satellite in Section 4, in

102 terms of geomagnetic activity dependence (Sec. 4.1) and frequency dependence (Sec. 4.2),

103 and the agreement and limitations of our model are discussed in Section 5. The major

104 findings of this work are summarized in Section 6.

2. The CRRES satellite and database

105 The Combined Release and Radiation Effects Satellite (CRRES) [*Johnson et al.*, 1992] is

106 particularly well-suited for the present study due to its favorable orbit and instrumentation

107 suite, and is used to provide information on the suprathermal electron fluxes, as well as

108 chorus wave intensities (discussed further in Section 4). The spacecraft was launched on

109 July 25, 1990 and operated in a highly elliptical geosynchronous transfer orbit with a

110 perigee of 305 km, an apogee of 35,768 km, and an inclination of 18°. The orbital period

111 was approximately 10 hours, and the initial apogee was at a magnetic local time (MLT)

112 of 0800 MLT. The magnetic local time of apogee decreased at a rate of approximately 1.3

113 hours per month until the satellite failed on October 11, 1991, when the apogee was at

114 approximately 1400 MLT. The satellite swept through the most important chorus source

115 region approximately 5 times per day, providing coverage for almost 15 months.

116 The suprathermal electron fluxes were measured by the Low Energy Plasma Analyzer

117 (LEPA). This instrument consisted of two electrostatic analyzers with microchannel plate

118 detectors, each with a field of view of $120° \times 5°$, one measuring electrons and the other

119 ions in the energy range 100 eV $< E <$ 30 keV [*Hardy et al.*, 1993]. The instrument

120 detected the complete pitch angle range from $0°$ to $180°$ every 30 sec with a resolution of

121 $5.625° \times 8°$ at 20 energy channels in the range 100 eV $< E <$ 30 keV. The chorus waves

122 were measured by the Plasma Wave Experiment (PWE) which detected the wave electric

123 field from 5.6 Hz to 400 kHz, using a 100 m tip-to-tip long wire antenna, with a dynamic

124 range covering a factor of at least 10^5 in amplitude [*Anderson et al.*, 1992].

125 In order to examine the global morphology of the suprathermal electron fluxes and the

126 chorus wave intensities as a function of geomagnetic activity we constructed a database

127 from the CRRES wave and particle observations. The wave data were initially corrected

128 for the instrumental background response and smoothed by using a running 3-min average

129 to take out the beating effects due to differences in the sampling and the spin rate.

130 Spurious data points, data spikes, and periods of instrumental downtime were flagged and

131 ignored in the subsequent statistical analyses. Twelve orbits, during which nontraditional

132 configurations were deployed for testing purposes, were also excluded from the analyses.

133 The electric field intensities, discussed in Section 4, together with the electron perpen-

134 dicular differential number flux for each energy level of the LEPA instrument were then

135 rebinned as a function of half orbit (outbound and inbound) and L in steps of $0.1L$.

136 The data were recorded together with the universal time (UT), magnetic latitude (λ_m),

137 magnetic local time (MLT), the AE index, and time spent in each bin with the same

138 resolution. The resulting database, consisting of plasma wave and particle measurements

139 from 939 orbits (1878 half orbits), was subsequently analyzed to determine the behavior

140 of the waves and the particles as a function of spatial location and magnetic activity.

141   Both whistler mode chorus and the suprathermal electrons tend to be observed outside

142   of the plasmapause. In order to exclude wave emissions and electron fluxes from inside the

143   plasmapause from the survey we adopt a criterion based on the amplitude of the waves in

144   the band $f_{ce} < f < 2f_{ce}$ following [*Meredith et al.*, 2004]. Waves in this frequency band,

145   which contain contributions from both electron cyclotron harmonic waves and thermal

146   noise, tend to be excluded from the high density region inside the plasmapause, and have

147   proven to be an excellent indicator of times when the satellite is outside the plasmapshere.

148   The specific criterion we adopt, based on a previous experimental study using data from

149   the CRRES Plasma Wave Experiment, requires that the wave amplitude for frequencies

150   in the range $f_{ce} < f < 2f_{ce}$ be greater than 0.0005 mVm^{-1} in order for the wave and

151   particle data to be included in the survey [*Meredith et al.*, 2004].

2.1. Suprathermal flux observations

152   Figure 1 shows the average distribution of perpendicular suprathermal electron fluxes

153   measured with LEPA on the CRRES satellite, averaged over a range of magnetic latitudes

154   within $\pm 15°$ of the magnetic equator. Each panel displays fluxes in color as a function

155   of L-shell and MLT, with the common colorbar shown at the bottom of the figure. The

156   fluxes are parameterized by energy channel and geomagnetic activity, showing (rows from

157   top to bottom) the 213 eV, 1.09 keV, 4.25 keV and 16.5 keV channels, for the magnetic

158   activity conditions (columns from left to right) AE < 100 nT, 100 < AE < 300 nT,

159   and AE > 300 nT. The statistical coverage of CRRES is shown at the bottom of each

160   column, as the number of samples in each L-MLT bin. These specific energy channels

161   have been chosen for a number of reasons: firstly, the range 0.213–16.5 keV was chosen

162   because the suprathermal electron energies responsible for Landau damping of chorus

163 waves fall comfortably within it, typically near ~ 1 keV [e.g., *Bortnik and Thorne*, 2006,

164 Fig. 3d]. Secondly, the choice of using only four of the energy channels available on

165 CRRES was made because it is the smallest number of points the gives a robust parameter

166 fit (discussed further below) and adding more data has little or no further effect upon the

167 fitted distribution, but only increases computation length. The spacing of energy channels

168 was chosen to be roughly even on a logarithmic scale, in both energy and velocity space

169 (see for example Figure 2).

170 The flux distributions show that suprathermal fluxes at all energies increase with in-

171 creasing geomagnetic activity, and penetrate to lower L-shells, due to the enhanced con-

172 vection electric field [e.g., *Korth et al.*, 1999]. The MLT distributions also become more

173 asymmetric with increasing geomagnetic activity, due to increases in both electron injec-

174 tion, and loss as they drift eastward around the Earth. Low energy (< 16 keV) electrons

175 are subject to strong diffusion loss during resonance with electrostatic electron cyclotron

176 harmonic (ECH) waves [*Horne and Thorne*, 2000] and whistler-mode chorus [*Glauert and*

177 *Horne*, 2005]. The loss timescale for strong diffusion is considerably shorter than the drift

178 timescale at these energies, giving rise to strong MLT gradients.

179 It should be noted that a few L-MLT bins do not contain particle data due to incomplete

180 coverage by CRRES (e.g., $4 < L < 5$, $2300 < $ MLT < 0000, and $L > 6$ at $0900 < $ MLT

181 < 1200). While we have taken measures to avoid most regions with insufficient coverage,

182 for example only considering the region $3 < L < 7$ in subsequent analysis, a few such

183 regions still remain. This problem has been addressed by smoothing and interpolating

184 the data in logarithmic space over the 2D plane. A number of different techniques of data

185 filling have been compared including more elaborate techniques [*Kondrashov and Ghil*,

186 2006], but since our data set is fairly smooth (particularly when the logarithm is used for

187 interpolation), the results obtained using the various methods agreed fairly well, and a

188 simple triangle interpolation scheme, using a gradient regularizer was chosen.

2.2. Parameter fitting

189 We aim to fit analytical functions representing the phase space density as a function

190 of velocity, $f(v)$, to the suprathermal flux observations shown in Figure 1, at every L,

191 and MLT bin. The fitted $f(v)$ functions can subsequently be used to calculate Landau

192 damping rates when combined with ray tracing. In order to illustrate our methodology, a

193 specific location is chosen, e.g., $L = 4.45$, MLT$= 5.5$, together with a geomagnetic activity

194 level, e.g., AE > 300 nT, giving the 4 measured flux values (J_{1-4}) corresponding to the

195 4 energy channels ($E_{1-4} = 0.213$, 1.09, 4.25, and 16.5 keV), illustrated as the diamond

196 symbols in Figure 2a. If an assumed distribution of the form:

$$J(E) = \frac{J_0}{E^m} \tag{1}$$

198 is used, the J_0 and m values can be readily obtained by taking the logarithm of (1),

$$\underbrace{\log_{10}(J_i)}_{y_i} = \underbrace{\log_{10}(J_0)}_{a_0} - \underbrace{m}_{a_1} \underbrace{\log_{10}(E_i)}_{x_i} \tag{2}$$

200 and solving for a_0, a_1 in (2) in a least-squares sense [*Press et al.*, 2002, p.661] where

201 (E_i, J_i) or (x_i, y_i), $i = 1 - 4$, are the data points. The overall goodness of fit is estimated

202 by the sum of squared residuals between the fitted curve and actual data points. The

203 least-squares fit described above is shown in Figure 2a as the solid, heavy line, with the

204 fit-parameters $J_0 = 2.14 \times 10^7$ cm^{-2}s^{-1}str^{-1}keV^{-1}, and $m = 0.755$. For comparison,

205 the data points are joined with a dashed line in Figure 2a, showing that the agreement

206 between data and fitted model is very good.

The flux $J(E)$ can be related to the phase space density $f(v)$ through the simple non-relativistic relation [*Walt*, 1994, p. 67]:

$$J(E) = \frac{v^2}{m'} f(v) \tag{3}$$

where v and m' are the electron velocity and mass respectively, but care must be exercised with regard to the selection of units. If the energy E is given in keV, and v in cms^{-1} as is conventionally done in cgs units, then:

$$m' = \kappa_0 m_e \tag{4}$$

where $m_e = 9.1 \times 10^{-31}$ kg, and $\kappa_0 = 6.25 \times 10^{11}$ C^{-1} is a unit correction factor. Using (3) and (4) we can translate the flux data points (J_i, E_i) to phase space density data points (v_i, f_i) as shown by the square symbols in Figure 2b.

If we further assume the phase space density expression to be of the form:

$$f(v) = \frac{A_N}{v^n} \tag{5}$$

as has been done previously [*Bell et al.*, 2002], then combining (1)–(5) gives:

$$n = 2a_1 + 2 \tag{6}$$

$$A_N = \frac{2 \times 10^{a_0}}{(\frac{1}{2}m')^{a_1 - 1}} \tag{7}$$

We show in Figure 2b the fitted distribution of 2a, translated to a phase space density function $f(v)$ in the form (5), with the fit parameters $n = 3.51$ and $A_N = 1.23 \times 10^3$ s^{3}cm^{-6}, where the data points are again joined by a dashed line which is completely obscured by the fitted distribution, indicating an excellent fit.

It should also be mentioned that we experimented with a phase space density of the form $f(v) = A_N/(v^2 + v_0^2)^{n/2}$, and fitted to the data points using a simulated annealing

algorithm [*Kirkpatrick et al.*, 1983], but in all cases the thermal velocity v_0 was found to

be negligible, so the simpler form (2) was used instead and fitted with the computationally

economical least-squares method.

3. Ray tracing and Landau damping

The fitted distribution discussed in Section 2.2 can now be combined with ray tracing to

study the propagation characteristics of chorus. We use the same methodology as *Bortnik*

et al. [2006], which is illustrated in Figure 3.

3.1. Ray tracing methodology

Using the Stanford VLF raytracer [*Inan and Bell*, 1977], individual rays representative

of chorus waves are injected at the magnetic equatorial plane ($\lambda = 0°$), with an initial

wave normal angle $\psi = 0°$, at a given L-shell, MLT, and frequency f which is normalized

to the equatorial gyrofrequency f_{ce}. For example, Figure 3a shows the propagation of a

single ray in the meridional plane, injected at $L = 4.45$, $\lambda = 0°$, $\psi = 0°$, and $f = 0.3f_{\mathrm{ce}}$.

In the course of the ray propagation, the appropriate suprathermal distribution $f(v)$ is

used to calculate the Landau damping rate at every point along the ray path [*Brinca*,

1972; *Bortnik et al.*, 2003], and integrated to give the total damping of the ray. Figure

3b shows the total damping calculated for the ray in panel (a), using the corresponding

distribution illustrated in Figure 2b (solid line) as a function of group time, together with

the latitude of the ray (dashed line). The point where the ray power reaches 1% of its

initial value is considered to be the termination of the wave, and the corresponding final

time τ_f and final latitude λ_f are indicated on the figure. In the present case shown in

248 Figure 3b, $\tau_f = 0.0971$ sec, $\lambda_f = 16.34°$, and in Figure 3a the ray path is only shown until

249 the termination point, also indicating the final propagation distance $d_f = 1.28 R_E$.

250   We note that the since we only have comprehensive information on perpendicular

251 suprathermal fluxes (Figure 1), the pitch-angle distribution is not known for all cases,

252 so it is assumed to be isotropic for simplicity. This assumption is consistent with past

253 work which has indicated that suprathermal fluxes are generally isotropic [*Bell et al.*,

254 2002], and even if some anisotropy is present, it does not affect the Landau damping rates

255 appreciably [*Thorne and Horne*, 1994]. The assumption of suprathermal flux isotropy

256 is particularly valid during active times (which are of most interest to us in the present

257 study) when the presence of intense waves tends to isotropise the electron distribution

258 [*Asnes et al.*, 2005] at lower energies.

259   In Figure 3c, the wave normal angle of the ray is shown as a function of latitude, to

260 the point of termination at $\lambda_f = 16.34°$. Even though the ray propagates for a relatively

261 short distance, it should be noted that the wave normal angle rotates to relatively high

262 values $\psi \sim 50°$ in the course of its lifetime, which accelerate its damping (c.f. Figure 3b)

263 [*Brinca*, 1972; *Thorne and Horne*, 1994].

264   We note that in Figure 3, and all subsequent ray tracing simulations in the present study,

265 the **B**-field model was assumed to be a simple dipole, and the equatorial gyrofrequency

266 f_{ce} is shown as the dashed line in Figure 3d. The equatorial number density was modeled

267 after *Carpenter and Anderson* [1992], with the plasmapause set at $L_{pp} \sim 2.5$ corresponding

268 to geomagnetic activity levels with $K_p^{\mathrm{max}} \sim 6.7$ (maximum value of K_p in the preceeding

269 24 hours). Off-equatorial values were calculated using the diffusive equilibrium model

270 [*Angerami and Thomas*, 1964].

3.2. Calculation results

The single ray example illustrated in Figure 3 can be repeated multiple times, in each case varying one of the initial parameters (e.g., L, MLT, AE, f, etc.), and the effect observed in the propagation parameters (e.g., τ_f, λ_f, d_f). The results of this analysis are shown in Figure 4, where the final latitude λ_f of each ray is plotted as a function of its initial L-shell and MLT, parameterized into 3 columns representing geomagnetic activity (corresponding to Figure 1), and 4 rows corresponding to the ray frequency normalized to the equatorial gyrofrequency (please note the colorbar is different for each row). The frequencies have been chosen to represent chorus rays ranging from the lowest observed values (row A, $f = 0.1f_{\mathrm{ce}}$), through typical lower band (row B, $f = 0.3f_{\mathrm{ce}}$) and upper band (row C, $f = 0.5f_{\mathrm{ce}}$), to the highest observed frequencies (row D, $f = 0.7f_{\mathrm{ce}}$). The initial wave normal angle was set to $\psi = 0°$ in all the simulations. The values at $L \sim 5 - 7$, MLT $\sim 0900 - 1200$ (indicated by the dashed oval in panel (Ab)) should be interpreted with caution since this region corresponds to interpolated fluxes (c.f. Figure 1, Section 2.1). The dark blue regions appearing at low L-shells in panels (Aa) and (Ac), MLT=1600 and 0600 respectively, correspond to rays that are able to undergo a magnetospheric reflection [e.g., *Parrot et al.*, 2003; 2004; *Bortnik et al.*, 2006] and return to low latitudes before being extinguished, due to the very low damping (corresponding to low frequency of the wave) and low L-shell, as discussed further below. Since our density profile was fixed in all simulations (e.g. Figure 3d), the expected average location of the plasmapause L_{pp} was marked explicitly in columns a and b, with $L_{\mathrm{pp}} \sim 5.1$ corresponding to $K_p^{\mathrm{max}} \sim 1$ in column a, $L_{\mathrm{pp}} \sim 3.75$ corresponding to $K_p^{\mathrm{max}} \sim 4$ in column b [*Carpenter and Anderson*, 1992], and $L_{\mathrm{pp}} = 2.5$ in column c as shown in Figure 3d. The chosen K_p^{max}

values are not necessarily proportional to the corresponding AE ranges, but are typical of quiet, moderately disturbed, and disturbed conditions, and are likely to be encountered in the given AE ranges. Since chorus is typically observed outside the plasmapause [e.g., *Anderson and Maeda*, 1977], only values at $L > L_{\mathrm{pp}}$ should be considered valid in the following discussion.

There are a number of features evident in Figure 4 which we discuss below. Firstly, in each panel it is evident that rays initiated at lower L-shells propagate to higher latitudes than those starting at higher L-shells, regardless of AE or f, for example in panel (Bc), $\lambda_f(L < 4) \sim 30°$ whereas $\lambda_f(L > 6) \sim 10°$. The same behavior (not shown) is also evident for the final propagation distance d_f, confirming that this is a real damping effect is not just a result of longer field-lines at higher L-shells. This behavior is related to the fact that damping rates are proportional to N_h/N_0 [*Brinca*, 1972], where N_h is the number of 'hot' particles, i.e., suprathermal flux, and N_0 is the background cold plasma density. Since convective injection of hot particles into the inner magnetosphere is more efficient at higher L than lower L, and cold plasma density is higher at lower L than at higher L (Figure 3d), the ratio N_h/N_0 is lower at lower L, corresponding to larger λ_f, and vice versa at higher L.

The second feature to note is that in all panels, independent of AE or f, the rays are completely damped while they are still propagating away from the equator, and thus (typically) do not magnetospherically reflect and return to the equator. This unidirectional propagation away from the equator has been well-noted in experimental studies [*LeDocq et al.*, 1998; *Lauben et al.*, 2002; *Santolik et al.*, 2004, 2005], and previously explained on the basis of Landau damping [*Bortnik et al.*, 2006] (though only a single hypothesized

suprathermal distribution was used in that case). In the present study, the unidirectional

propagation of chorus is confirmed using measured, local flux distributions.

The MLT distribution of λ_f exhibits a distinct progression at all frequencies when

geomagnetic activity is increased from quiet times (column a) to disturbed times (column

c). For example, examining λ_f at a location of +1 L-shell outside the plasmapause,

in panel (Ba) it is clear that $\lambda_f(L = 6) \sim 15°$ and relatively independent of MLT,

with perhaps slightly increased values near midnight. Comparing to panel (Bc), $\lambda_f(L = 3.5, \text{MLT}= 0000) \sim 27°$, and $\lambda_f(L = 3.5, \text{MLT}= 1200) \sim 40°$, there is a pronounced MLT

dependence at all L and f, with low values near midnight, increasing with MLT towards

noon, peaking postnoon and returning to low values again at night. This geomagnetically

controlled MLT dependence is related to the drift and loss timescales of suprathermal

electrons which ultimately control the damping of the chorus waves, and will be discussed

further in Section 5.

Finally, we note that λ_f is strongly frequency dependent, regardless of AE, MLT or

L-shell. Lower frequency components (row A) propagate furthest, with λ_f decreas-

ing as the frequency is increased (e.g., row D). For example, at $L = 4$, MLT=1200,

AE> 300 nT, $\lambda_f(f = 0.1f_{\text{ce}}) \sim 56°$, $\lambda_f(f = 0.3f_{\text{ce}}) \sim 28°$, $\lambda_f(f = 0.5f_{\text{ce}}) \sim 15°$, and

$\lambda_f(f = 0.7f_{\text{ce}}) \sim 7.5°$. The tendency of higher frequencies to Landau damp more severely

has been previously noted [*Thorne and Horne*, 1994; *Bortnik et al.*, 2003] in relation to

magnetospherically reflected whistler propagation studies, and is due to the combination

that (i) higher frequency waves resonate with lower energy electrons which are more abun-

dant (and have larger values of $\partial f / \partial v_{||}$), and (ii) that higher frequency waves also rotate

338 faster to the resonance cone, which which is at lower angles than for lower frequency

339 waves.

4. Comparison to observations

340   In order to compare our simulated results to observations we use the CRRES wave

341 data, processed and rebinned as described in Section 2. Only the wave data inferred to be

342 outside the plasmapause are included, by adopting the criterion that the wave amplitude

343 for frequencies in the range $f_{ce} < f < 2f_{ce}$ must be greater than 0.0005 mVm^{-1} [e.g.,

344 *Meredith et al.*, 2004]. For the present comparison, the chorus wave intensities were defined

345 by integrals of the averaged wave spectral density (V^2 m^{-2} Hz^{-1}) over the frequency range

346 $0.1f_{ce} < f < 1.0f_{ce}$ in steps of $0.1f_{ce}$, where f_{ce} is the equatorial electron gyrofrequency

347 as above. The gyrofrequency f_{ce} was determined from the local ambient magnetic field

348 determined from the fluxgate magnetometer instrument [*Singer et al.*, 1992] assuming a

349 dipole field.

4.1. Dependence on geomagnetic activity

350   In Figure 5 we show the chorus wave power binned as a function of L-shell and MLT,

351 paramterized by magnetic latitude range (rows 1–3: $|\lambda_m| > 20°$, $10° < |\lambda_m| < 20°$,

352 $|\lambda_m| < 10°$) and geomagnetic activity (columns 1–3: AE < 100 nT, $100 <$ AE < 300

353 nT, and AE > 300 nT). The two lowest frequency components are shown, since these are

354 expected to experience the least amount of damping (c.f., Figure 4). The 9 panels on

355 the left correspond to the frequency range $0.1f_{ce} < f < 0.2f_{ce}$ and the 9 on the right to

356 $0.2f_{ce} < f < 0.3f_{ce}$, with a dashed line showing the separation.

357   Immediately evident is the strong degree of geomagnetic control of chorus intensity.

358   During active times (column 3), the chorus wave power is ~ 1000 times stronger than

359   during quiet times (column 1), since the energetic particles that drive chorus emissions

360    $(E \sim 10 - 100$ keV) are only injected when strong convection electric fields are present

361   during active conditions [*Smith et al.*, 1999, 2004; *Collier and Hughes*, 2004a,b]. The MLT

362   dependence during quiet times is weak, in agreement with our theoretical predictions.

363   During active times, there is a pronounced MLT dependence: at low latitudes, mid-

364   latitudes, and high latitudes the chorus wave power is observed predominantly at $\mathrm{MLT_{low\lambda}}$

365    $\sim 2300 - 0800$, $\mathrm{MLT_{mid\lambda}} \sim 0100 - 1400$, and $\mathrm{MLT_{high\lambda}} \sim 0700 - 1500$ respectively (for

366    $0.2f_{\mathrm{ce}} < f < 0.3f_{\mathrm{ce}}$). There is a clear tendency of the wave power to progressively

367   shift to high latitudes as MLT is increased, in direct agreement with our 'active time'

368   calculations (Figure 4, column c). Beyond MLT ~ 1500 the chorus power abruptly drops

369   off, presumably due to the loss of the energetic electrons which are the source of the waves.

4.2. Storm-time chorus distributions

370   In Figure 6 we show the distribution of chorus wave power for active conditions (i.e.,

371   column 3 of Figure 4, AE > 300 nT), parameterized by magnetic latitude range (rows

372   1–3: $|\lambda_m| > 20°$, $10° < |\lambda_m| < 20°$, $|\lambda_m| < 10°$) and frequency band, normalized to the

373   equatorial electron cyclotron frequency (columns 1–6: $f/f_{\mathrm{ce}} = $ 0.1–0.2, 0.2–0.3, 0.3–0.4,

374   0.4–0.5, 0.5–0.6, and 0.6–0.7).

375   The tendency of chorus wave power to move to higher latitudes with increasing MLT is

376   clearly evident at all frequency ranges, in agreement with our calculations. In addition, if

377   we contrast a low frequency component (e.g., column 2, $0.2f_{\mathrm{ce}} < f < 0.3f_{\mathrm{ce}}$), with a high

378   frequency component (e.g., column 5, $0.5f_{\mathrm{ce}} < f < 0.6f_{\mathrm{ce}}$), it is clear that significantly

379 less power is able to propagate to high latitudes when the frequency is high, compared

380 to when the frequency is low. This supports our theoretical prediction that Landau

381 damping controls the latitude to which chorus waves are able to propagate, indicating

382 larger damping at higher frequencies.

383 By studying the L-shell distribution of the wave power, for example row 2, columns

384 4–6, it is apparent that the chorus wave power is able to propagate to higher latitudes at

385 lower L-shells, in accordance with our prediction. We note that the ability to observe this

386 L-shell distribution is also consistent with our model, and should only be evident above

387 $f \sim 0.5 f_{\mathrm{ce}}$ where λ_f falls in the range $10° - 20°$ (c.f., Figure 4), whereas lower frequency

388 components have $\lambda_f > 20°$ for most of the L-shells under study, which all fall into the

389 highest latitude bin observed by CRRES. The fact that chorus wave power is observed

390 only outside of $L \sim 3$ is attributed to the location of the plasmapause.

5. Discussion

391 In the foregoing comparison, it was demonstrated that many of the observed character-

392 istics of the chorus wave-power distribution could be successfully explained on the basis

393 of Landau damping by the suprathermal electron (~ 1 keV) population. In particular,

394 the tendency of lower frequency components to propagate to higher latitudes than higher

395 frequency components was clearly shown in both our simulations and the CRRES data.

396 The fact that chorus waves are Landau damped during their first hop away from the

397 equator (unidirectional propagation) support previous theoretical [*Bortnik et al.*, 2006]

398 and observational [*LeDocq et al.*, 1998; *Lauben et al.*, 2002] studies (although a few obser-

399 vations of weak, magnetospherically reflected chorus have been made [*Maeda and Smith*,

400 1981; *Parrot et al.*, 2003; 2004]), and the approximate final latitude to which various fre-

401 quencies propagated was consistent with the CRRES data. The tendency of chorus waves

402 to propagate to larger λ_f at lower L-shells was predicted in our simulations and observed

403 in the CRRES data.

404   Of particular interest was the agreement in the MLT distribution of chorus wave power,

405 as observed at various latitudinal ranges. In both our theoretical predictions and CRRES

406 data it was shown that chorus waves tend to be more confined to low latitudes on the

407 nightside. The accessible latitude range of chorus increases with MLT, and peaks on the

408 dayside. This propagation characteristic was attributed purely to the behavior of the

409 suprathermal flux distribution.

410   In Figure 7 the controlling influence of the suprathermal electron distribution upon

411 wave propagation is demonstrated, by plotting the fitted flux distribution (1) at $L = 4.85$

412 as a function of MLT and E (Figure 7e), where the region MLT=1000-1100 corresponds

413 to incomplete CRRES coverage. The ray paths (plotted from initiation to their respective

414 termination points) at 4 selected MLT locations are shown in Figures 7a-d, corresponding

415 to MLT = 3.5, 9.5, 15.5 and 21.5 respectively. The flux fitting parameters J_0 and m

416 (Eqn. (1)) are shown in Figures 7f,g and the corresponding phase space density fitting

417 parameters A_N and n are shown in Figures 7h,i.

418   Figure 7e shows that $J(E)$ varies strongly as a function of MLT. When J(E) is most

419 intense, Landau damping is the most severe and propagation latitudes are the shortest

420 (Figure 7a). As MLT increases, $J(E)$ is decreased due to scattering and loss by a number of

421 plasma waves (including chorus) [*Korth et al.*, 1999; *Horne et al.*, 2003; *Chen et al*, 2005]

422 and propagation lengths increase (Figure 7b), reaching a maximum at postnoon MLT

423 (Figure 7c). Thereafter, $J(E)$ again increases towards the nightside with corresponding

424 increase in damping (Figure 7d).

425   Our interpretation of the flux decrease is illustrated schematically in Figure 7j, which

426 shows the convective injection of suprathermal electrons from the plasmasheet, followed by

427 a combination of gradient-curvature, and $\mathbf{E} \times \mathbf{B}$ drift which causes the electrons to drift

428 in an eastward direction around the Earth. During their drift trajectories, the electrons

429 experience scattering by a variety of plasma waves which cause losses on a timescale

430 comparable to the strong diffusion lifetime [*Horne and Thorne*, 2000; *Glauert and Horne*,

431 2005] which is shorter than the drift period of the electrons, and hence the suprathermal

432 electron population is not able to complete a full drift around the Earth (on average).

433 Moreover, by examining Figures 7f and 7g (or alternatively Figures 7h and 7i), it is clear

434 that not only the absolute value of the flux, J_0, is decreased, but the spectrum becomes

435 steeper since m progressively increases with MLT. This indicates that electrons with $E < 1$

436 keV and $E > 1$ keV experience different scattering rates relative to their drift timescales,

437 with the higher energy electrons being scattered faster than the lower energy electrons.

438 The steepening of the spectrum $J(E)$ slightly increases damping rates with MLT, but

439 is dominated by the decrease in J_0 which drives damping rates to very low values. The

440 tendency of lower energy electrons to propagate further in MLT is shown schematically

441 in Figure 7j.

442   Even though many propagation characteristics of chorus are successfully reproduced

443 by our model, there are a few limitations which warrant discussion. Firstly, in all our

444 simulations only the relative power of each ray was considered (Figure 3b), which implicitly

445 assumes a uniform source of chorus waves, and neglects any inherent MLT variation in

the source. This difference becomes apparent in comparing our simulation (e.g., Figure 4, panel Bc, $L > 5$) with the observations (e.g., Figure 6, column 3) where it is clear that chorus wave power drops off dramatically beyond MLT ~ 1500, whereas the simulations show the λ_f continues to increase until MLT ~ 1800. This difference is attributed to the fact that the flux of electrons responsible for the generation of chorus $E \sim 10 - 100$ keV is not uniformly distributed in MLT, but also drifts around the Earth and is scattered by various waves, decreasing both its absolute flux levels, as well as decreasing the anisotropy in the pitch-angle distribution which is presumably the source of free-energy that creates the chorus waves [*Burton*, 1976]. By the time the source electrons reach MLT ~ 1500 there is insufficient flux and anisotropy to drive chorus generation and the wave power drops off dramatically, even though propagation lengths remain high, implying that if there were any chorus waves being generated, they would have propagated to large latitudes.

Secondly, in our simulations we have assumed that chorus waves are generated in a field-aligned $\psi = 0°$ direction, due to the fact that cyclotron growth rates are maximized, and Landau damping rates are minimized in this configuration [*Kennel*, 1966; *Brinca*, 1972]. In addition, many observational studies have indicated that chorus is indeed observed to be predominantly field-aligned near its source [*Burton and Holzer*, 1974; *Goldstein and Tsurutani*, 1984]. While there is evidence of whistler wave-power leaking into a spectrum of non-zero wave normal angles [*Lauben et al.*, 2002; *Chum and Santolik*, 2005; *Santolik et al.*, 2006; *Platino et al*, 2006], it appears that the bulk of the wave power is indeed initiated in a field-aligned orientation, and the observed large-scale characteristics reported in this paper are consistent with this generation regime.

Finally, we note that in our simulation we have assumed that chorus waves are instantaneously produced at the geomagnetic equator and then propagate away, which is an overly simplistic treatment of the chorus generation problem [a very complicated problem indeed! e.g., *Helliwell*, 1967, 1995; *Omura et al.*, 1991; *Hattori et al.*, 1991; *Sazhin and Hayakawa*, 1992; *Trakhtengerts*, 1995, 1999; *Nunn et al.*, 1997]. An example of source dynamics can be seen in Figure 6, e.g., columns 1 and 2, where the chorus wave power is seen to be relatively weak on the dayside at $|\lambda_m| < 10°$, and increases with latitude, reaching a maximum at $|\lambda_m| > 20°$. This distribution of wave power has led some authors to suggest that the chorus generation region could be located at high latitudes on the dayside [*Tsurutani and Smith*, 1977] but recent studies of Poynting flux show that even though wave power maximises at high latitudes on the dayside, the propagation direction is uniformly away from the equator at all MLT [*LeDocq et al.*, 1998; *Lauben et al.*, 2002; *Santolik et al.*, 2004, 2005]. A possible interpretation of this behavior based on quasilinear theory, is that the cyclotron growth rates responsible for the generation of chorus become progressively lower with increasing MLT, due to the scattering (loss) and isotropization of the source population of electrons $E \sim 10 - 100$ keV. To reach a given amplitude (in order to reach the nonlinear threshold), the chorus waves need to propagate for a longer distance due to the lower cyclotron growth rate, which is made possible by the concomitant decrease in the Landau fluxes and resultant increase in λ_f (Figure 4), as well as decreased field-line inhomogeneity on the dayside [*Tsyganenko and Sitnov*, 2005] allowing more uniform wave propagation. The above interpretation is consistent with the fact that it is predominantly the lower frequencies which show the extended growth region. Since lower frequency waves resonate with higher energy electrons, which are far

less numerous than lower energy electrons, it is the lower frequencies which will have the

lowest growth rates and hence require the largest propagation distance to achieve signif-

icant total amplification. Wave power density increase is also enhanced due to magnetic

field line convergence at high latitudes.

6. Conclusions

In the present paper, statistical distributions of suprathermal electrons ($E = 0.213 - 16.5$

keV) from the CRRES satellite were used to fit analytical phase space density distributions

of the form $f(v) = A_N/v^n$, as a function of L-shell, MLT, and geomagnetic activity. These

fitted distributions were then used in conjunction with ray tracing to calculate the Landau

damping rates of an ensemble of rays representing chorus waves. The modeled propagation

characteristics were compared to statistical observations of chorus wave power, also from

the CRRES satellite, in various frequency bands ($f/f_{\mathrm{ce}} = 0.1 - 0.2, 0.2 - 0.3, ..., 0.6 - 0.7$),

latitude ranges ($|\lambda_m| < 10°$, $10° < |\lambda_m| < 20°$, and $|\lambda_m| < 20°$), and under a variety of

geomagnetic conditions (AE < 100 nT, $100 <$ AE < 300 nT, and AE > 300 nT).

Based on the work presented in this paper, a number of conclusions can be drawn:

1. At all wave frequencies and geomagnetic activity conditions, chorus rays were Landau

damped before they were able to magnetospherically reflect, consistent with the observed

unidirectional propagation observed generally away from the equator.

2. Chorus rays propagated to larger latitudes at lower L-shells (but outside the plasma-

pause) than at larger L-shells, due to the lower ratio of N_h/N_0 (number of 'hot' electrons

relative to the cold background electron number density).

3. Lower frequency rays were found to propagate to higher latitudes than higher frequency rays, consistent with CRRES observations. In addition, there was good agreement between the absolute value of the final latitudes predicted by our model and the inferred final latitude from the CRRES observations.

4. The MLT distribution of chorus wave power was found to be relatively uniform or unstructured during geomagnetically quiet conditions, but showed a pronounced asymmetry during active conditions, with small propagation latitudes on the nightside, and large propagation latitudes on the dayside. This asymmetry was well reflected in the CRRES observations.

5. The MLT distributions of chorus wave power under active conditions were found to be strongly controlled by the underlying distribution of suprathermal electrons, which were most intense on the nightside resulting in the most severe damping, and gradually decayed towards the dayside where large propagation lengths were observed. This depletion of suprathermal particles was interpreted on the basis of the loss timescales being faster than drift timescales, with the higher energy particles being affected more than the lower energy electrons.

It was shown that many characteristics of the chorus wave-power distribution in L, MLT, and latitude, were explained very well on the basis of Landau damping by the suprathermal particle population. This important population of particles may thus be indirectly responsible for controlling the dynamics of the relativistic radiation-belt electrons, since many of the theories of chorus acceleration and loss rely on the interaction between chorus waves and energetic particles at mid- and high- latitudes [*Horne et al.*, 2005b; *Thorne et al.*, 2005a,b].

It was also shown that certain features appear in the chorus wave distribution on the dayside, which are almost certainly related to the dynamics of the energetic electrons $E \sim 10 - 100$ keV responsible for the generation of the chorus waves. Although we have proposed a preliminary reason for this behavior, it remains to be treated in a more quantitative way in future studies.

References

Abel, G. A., M. P. Freeman, A. J. Smith, and G. D. Reeves (2006), Association of substorm chorus events with drift echos, *J. Geophys. Res.*, Vol. 111, Iss. A11, doi:10.1029/2006JA011860.

Anderson, R. R., D. A. Gurnett, and D. L. Odem (1992), CRRES plasma wave experiment, *J. Spacecr. Rockets, 29*, 570.

Anderson, R. R. and K. Maeda (1977), VLF emissions associated with enhanced magnetospheric electrons, *J. Geophys. Res.*, Vol. 82, pp. 135-146.

Angerami, J.J., and J.O. Thomas (1964), Studies of Planetary Atmospheres. 1. Distribu-
    tion of Electrons + Ions in Earths Exosphere, *J. Geophys. Res.*, 69 (21), 4537.

Asnes, A, J. Stadsnes, R. W. Friedel, N. Ostgaard, and M. Thomsen (2005), Medium
    energy pitch angle distribution during substorm injected electron clouds, *Geophys. Res.
    Lett.*, Vol. 32, Iss. 10, doi:10.1029/2004GL022008.

Bell, T.F., U.S. Inan, J. Bortnik, and J.D. Scudder (2002), The Landau damping of
    magnetospherically reflected whistlers within the plasmasphere, *Geophys. Res. Lett.*,
    Vol. 29, No. 15.

Bortnik, J., U.S. Inan, and T.F. Bell (2003), Energy distribution and lifetime of magne-
    tospherically reflecting whistlers in the plasmasphere, *J. Geophys. Res.*, Vol. 108, No.
    A5.

Bortnik, J. and R. M. Thorne (2006), The dual role of ELF/VLF chorus waves in the
    acceleration and precipitation of radiation belt electrons, *J. Atmos. Sol. Terr. Phys.*,
    [in print].

Bortnik J., U. S. Inan, and T. F. Bell (2006), Landau damping and resultant
    unidirectional propagation of chorus waves, *Geophys. Res. Lett.*, Vol. 33, Iss. 3,
    doi:10.1029/2005GL024553.

Brinca, A.L. (1972), On the Stability of Obliquely Propagating Whistlers, *J. Geophys.
    Res.*, Vol. 77, No. 19, p. 3495.

Burtis, W. J., and Helliwell, R. A. (1969), Banded chorus – a new type of VLF radiation
    observed in the magnetosphere by OGO 1 and OGO 3, *J. Geophys. Res.*, Vol. 74, 3002.

Burtis, W.J., and Helliwell, R.A. (1976), Magnetospheric chorus: Occurrence patterns
    and normalized frequency, *Planet. Space Sci.*, Vol. 24, No. 11, p. 1007-1007.

577 Burton R.K., and R.E. Holzer (1974), The origin and propagation of chorus in the outer

578   magnetosphere, *J. Geophys. Res.*, Vol. 79, No. 7, pp. 1014-1023.

579 Burton, R. K. (1976), Critical electron pitch angle anisotropy necessary for chorus gener-

580   ation, *J. Geophys. Res.*, Vol. 81, pp. 4779-4781.

581 Carpenter, D.L., and R.R. Anderson (1992), An ISEE/Whistler Model of Equatorial

582   Electron-Density in the Magnetosphere, *Journal of Geophysical Research-Space Physics*,

583   97 (A2), 1097-1108.

584 Chen, M.W., M. Schulz, P.C. Anderson, G. Lu, G. Germany, and M. Wüest (2005),

585   Storm time distributions of diffuse auroral electron energy and X-ray flux: Compar-

586   ison of drift-loss simulations with observations, *J. Geophys. Res.*, Vol. 110, A03210,

587   doi:10.1029/2004JA010725.

588 Collier, A., and A. Hughes (2004a), Modeling substorm chorus events in terms of dispersive

589   azimuthal drift, *Annales Geophysicae*, Vol. 22, Iss. 12, pp. 4311-4327.

590 Collier, A., and A. R. W. Hughes (2004b), Modeling and analysis of substorm related

591   chorus events, *Adv. in Space Res.*, Vol. 34, Iss. 8, pp. 1819-1823.

592 Chum, J. and O. Santolik (2005), Propagation of whistlere-mode chorus to low altitudes:

593   divergent ray trajectories and ground accessibility, *Annales Geophysicae*, Vol. 23, Iss.

594   12, pp. 3727-3738.

595 Goldstein B.E., and B.T. Tsurutani (1984), Wave normal directions of chorus near the

596   equatorial source region, *J. Geophys. Res.*, Vol. 89, No. A5, pp. 2789-2810.

597 Hardy, D. A., D. M. Walton, A. D. Johnstone, M. F. Smith, M. P. Gough, A. Huber, J.

598   Pantazis, and R. Burkhardt (1993), Low energy plasma analyser, *IEEE Trans. Nucl.*

599   *Sci., 40*, 246.

Hattori, K., M. Hayakawa, D. Lagoutte, M. Parrot, and F. Lafeuvre (1991), Further evidence of triggering chorus emissions from the wavelets in the hiss band, *Planet. and Space Sci.*, Vol. 39, Iss. 11, pp. 1465-1472.

Helliwell, R.A. (1965), *Whistlers and related ionospheric phenomena*, Stanford University Press, Stanford, Calif.

Helliwell, R.A. (1967), A Theory of Discrete VLF Emissions from Magnetosphere, *Journal of Geophysical Research*, 72 (19), 4773-4790.

Helliwell, R. A. (1995), The role of the Gendrin mode of VLF propagation in the generation of magnetospheric emissions, *Geophys. Res. Lett*, Vol. 22, Iss. 16, pp. 2095–2098, doi:10.1029/95GL02003.

Horne, R. B., and R. M. Thorne (1998), Potential waves for relativistic electron scattering and stochastic acceleration during magnetic storms, *Geophys. Res. Lett.*, 25, 3011.

Horne, R. B., and R. M. Thorne (2000), Electron pitch angle diffusion by electrostatic electron cyclotron harmonic waves: the origin of pancake distributions, *J. Geophys. Res.*, Vol. 105, Iss. A3, pp. 5391–5402, doi:10.1029/1999JA900447.

Horne, R. B., and R. M. Thorne (2003), Relativistic electron acceleration and precipitation during resonant interactions with whistler mode chorus *Geophys. Res. Lett.*, 30, 1527.

Horne, R. B., R. M. Thorne, Y. Y. Shprits, N. P. Meredith, S. A. Glauert, A. J. Smith, S. G. Kanekal, D. N. Baker, M. J. Engebretson, J. L. Posch, M. Spasojevic, U. S. Inan, J. S. Pickett, and P. M. E. Decreau (2005a), Wave acceleration of electrons in the Van Allen radiation belts, *Nature*, Volume 437, Issue 7056, pp. 227-230, doi: 10.1038/nature03939.

Horne, R. B., R. M. Thorne, S. A. Glauert, J. M. Albert, N. P. Meredith, and R. R. Anderson (2005b), Timescale for radiation belt electron acceleration by whistler mode

623   chorus waves, *J. Geophys. Res.*, Vol. 110, A03225, doi:10.1029/2004JA010811.

624   Horne, R. B., N. P. Meredith, S. A. Glauert, A. Varotsou, R. M. Thorne, Y. Y. Shprits,

625   and R. R. Anderson (2006), Mechanisms for the acceleration of radiation belt electrons,

626   in *Recurrent Magnetic Storms: Corotating Solar Wind Streams, Geophys. Monogr. Ser.*,

627   vol. 167, edited by B. T. Tsurutani, R. L. McPherron, W. D. Gonzalez, G. Lu, J. H.

628   Sobral, and N. Gopalswarmy pp 151-173, AGU, Washington, D.C.

629   Inan, U.S., and T.F. Bell (1977), The Plasmapause as a VLF Wave Guide, *J. Geophys.*

630   *Res.*, Vol. 82, No. 19, 2819-2827.

631   Johnson, M. H., and J. Kierein (1992), Combined release and radiation effects satellite

632   (CRRES) - spacecraft and mission, *Journal of Spacecraft and Rockets*, Vol. 29, No. 4,

633   pp. 556–563.

634   Kennel, C. (1966), Low-Frequency Whistler Mode, *Phys. Fluids*, Vol. 9, No. 11.

635   Kennel, C. F., and R. M. Thorne (1967), Unstable growth of unducted whistlers propa-

636   gating at an angle to the geomagnetic field, *J. Geophys. Res.*, Vol. 72, p. 871.

637   Kirkpatrick, S., C. D. Gelatt Jr., and M. P. Vecchi (1983), Optimization by simulated

638   annealing, *Science*, Vol. 220, No. 4598.

639   Kondrashov, D., and M. Ghil (2006), Spatio-temporal filling of missing data points in

640   geophysical data sets, *Nonlin. Proccesses Geophys.*, 13, pp. 151-159.

641   Korth, H., M.F. Thomsen, J.E. Borovsky, and D.J. McComas (1999), Plasma sheet access

642   to geosynchronous orbit, *J. Geophys. Res.*, Vol. 104, No. A11, pp. 25,047-25,061.

643   Koons, H.C., and J.L. Roeder (1990), A survey of equatorial magnetospheric wave activity

644   between 5 and 8 R_{E}, *Planet. Space Sci.*, Vol. 38, No. 10, pp. 1335-1341.

Lauben, D.S., U.S. Inan, T.F. Bell, and D.A. Gurnett (2002), Source char-
    acteristics of ELF/VLF chorus, *J. Geophys. Res.*, Vol. 107, No. A12, 1429,
    doi:10.1029/2000JA003019.

LeDocq, M.J., D.A. Gurnett, and G.B. Hospodarsky (1998), Chorus source locations from
    VLF Poynting flux measurements with the Polar spacecraft, *Geophys. Res. Lett.*, Vol.
    25, No. 21, pp. 4063-4066.

Lubchich, A. A., A. G. Yahnin, E. E. Titova, A. G. Demekhov, V. Yu. Trakhtengerts,
    J. Manninen, and T. Turunen (2006), Longitudinal drift of substorm electrons as the
    reason of impulsive precipitation events and VLF emissions, *Annales Geophysicae*, 24,
    pp. 2667–2684.

Lyons, L. R., D.-Y. Lee, R. M. Thorne, R. B. Horne, and A. J. Smith (2005), Solar wind-
    magnetosphere coupling leading to relativistic electron energization during high-speed
    streams, *J. Geophys. Res.*, Vol. 110, Iss. A11, doi:10.1029/2005JA011254.

Maeda, K, and P. H. Smith (1981), VLF emissions associated with ring current electrons:
    off equatorial observations, *Planet. Space Sci.*, Vol. 29, Iss. 8, p. 825-835.

Meredith, N. P., R. B. Horne, and R. R. Anderson (2001), Substorm dependence of
    chorus amplitudes: Implications for the acceleration of electrons to relativistic energies,
    J. Geophys. Res., Vol. 106, No. A7, pp. 13,165-13,178.

Meredith, N. P., R. B. Horne, D. Summers, R. M. Thorne, R. H. A. Iles, D. Heynder-
    ickx and R. R. Anderson (2002a), Evidence for acceleration of outer zone electrons to
    relativistic energies by whistler mode chorus, *Ann. Geophys., 20*, 967.

Meredith N. P., R. B. Horne, R. H. A. Iles, R. M. Thorne, D. Heynderickx, and R. R. An-
    derson (2002b), Outer zone relativistic electron acceleration associated with substorm-

enhanced whistler mode chorus, *J. Geophys. Res.*, 107 (A7), doi:10.1029/2001JA900146.

Meredith, N. P., R. B. Horne, R. M. Thorne, and R. R. Anderson (2003a), Favored regions for chorus-driven electron acceleration to relativistic energies in the Earth's outer radiation belt, *Geophy. Res. Lett.*, Vol. 30, No. 16, p. 1871, doi:10.1029/2003GL017698.

Meredith N. P., M. Cain, R. B. Horne, R. M. Thorne, D. Summers, R. R. Anderson (2003b), Evidence for chorus-driven electron acceleration to relativistic energies from a survey of geomagnetically disturbed periods, *J. Geophys. Res.*, 108 (A6), 1248, doi:10.1029/2002JA009764.

Meredith, N. P., R. B. Horne, R. M. Thorne, D. Summers, and R. R. Anderson (2004), Substorm dependence of plasmaspheric hiss, *J. Geophys. Res.*, Vol. 109, A06209, doi:1029/2004JA010387.

Miyoshi Y., A. Morioka, H. Misawa, T. Obara, T. Nagai, and Y. Kasahara (2003), Rebuilding process of the outer radiation belt during the 3 November 1993 magnetic storm: NOAA and Exos-D observations, *J. Geophys. Res.*, Vol. 108, Iss. A1, doi:10.1029/2001JA007542.

Nunn, D., Y. Omura, H. Matsumoto, I. Nagano, and S. Yagitani (1997), The numerical simulation of VLF chorus and discrete emissions observed on the Geotail satellite using a Vlasov code, *J. Geophys. Res.*, Vol. 102, Iss. A12, p. 27083-27098.

Omura, Y., D. Nunn, H. Matsumoto, and M. J. Rycroft (1991), A review of observational, theoretical, and numerical studies of VLF triggered emissions, *J. Atmos. and Terr. Phys.*, 53, pp. 351–368.

Parrot, M., O. Santolik, D. Gurnett, J. Pickett, and N. Cornilleau-Wehrlin (2004), Characteristics of magnetospherically reflected chorus waves observed by CLUSTER, *Annales*

691 *Geophysicae*, Vol. 22, Iss. 7, pp. 2597-2606.

692 Parrot, M., O. Santolik, N. Cornilleau-Wehrlin, M. Maksimovic, and C. Harvey (2003),

693 Magnetospherically reflected chorus waves revealed by ray tracing with CLUSTER data,

694 *Annales Geophysicae*, Vol. 21, Iss. 5, pp. 1111-1120.

695 Platino, M., U. S. Inan, T. F. Bell, J. S. Pickett, and P. Canu (2006), Rapidly moving

696 sources of upper band ELF/VLF chorus near the magnetic equator, *J. Geophys. Res.*,

697 Vol. 11, Iss. A9. doi:10.1029/JA011468.

698 Press W. H., S. A. Teukolsky, W. T. Vetterling, and B. P. Flannery (2002), *Numerical*

699 *Recipes in C*, Cambridge University Press.

700 Santolik, O., D. A. Gurnett (2003), Transverse dimensions of chorus in the source region,

701 *Geophys. Res. Lett.*, Vol. 30, Iss. 2, pp. 3-1, CiteID 1031, DOI 10.1029/2002GL016178.

702 Santolik, O., D.A. Gurnett, and J.S. Pickett (2004), Multipoint investigation of the source

703 region of storm-time chorus, *Annales Geophysicae*, 22, pp. 2555-2563.

704 Santolik, O., D.A. Gurnett, J.S. Pickett, M. Parrot, N. Cornilleau-ehrlin, (2005), Central

705 position of the source region of storm-time chorus, *Planetary and Space Science*, 53, pp.

706 299-305.

707 Santolik, O., J. Chum, M. Parrot, D. A. Gurnett, J. S. Pickett, and N. Cornilleau-Wehrlin

708 (2006), Propagation of whistler mode chorus to low altitudes: Spacecraft observations

709 of structured ELF hiss, *J. Geophys. Res.*, Vol. 111, Iss. A10, doi:10.1029/2005JA011462.

710 Sazhin, S.S., and M. Hayakawa, (1992) Magnetospheric chorus emissions: a review, *Plan-*

711 *etary and Space Science*, vol. 40, no. 5, p.681-697.

712 Shprits, Y. Y., R. M. Thorne, R. B. Horne, S. A. Glauert, M. Cartwright, C. T. Russell,

713 D. N. Baker, and S. G. Kanekal (2006), Acceleration mechanism responsible for the

714   formation of the new radiation belt during the 2003 Halloween solar storm, *Geophys.*

715   *Res. Lett.*, Vol. 33, No. 5, CiteID L05104.

716   Singer, H. J., W. P. Sullivan, P. Anderson, F. Mozer, P. Harvey, J. Wygant, and W. McNeil

717   (1992), Fluxgate magnetometer instrument on the CRRES, *J. Spacecr. Rockets, 29*, 599.

718   Smith, A. J., M. P. Freeman, M. G. Wickett, and B. D. Cox (1999), On the relationship

719   between the magnetic and VLF signatures of the substorm expansion phase, *J. Geophys.*

720   *Res.*, Vol. 104, No. A6, pp. 12,351–12,360.

721   Smith, A. J., R. B. Horne, and N. P. Meredith (2004), Ground observations

722   of chorus following geomagnetic storms, *J. Geophys. Res.*, Vol. 109, A02205,

723   doi:10.1029/2003JA010204.

724   Spasojevic, M., Inan, U. S. (2005), Ground based VLF observations near L = 2.5 during

725   the Halloween 2003 storm, *Geophys. Res. Lett.*, Vol. 32, Iss. 21, CiteID L21103.

726   Storey, L.R.O., (1953) An investigation of whistling atmospherics, *Phil. Trans. Roy. Soc.*

727   246, 113.

728   Summers D., R. M. Thorne, and F. Xiao (1998), Relativistic theory of wave-particle

729   resonant diffusion with application to electron acceleration in the magnetosphere, *J.*

730   *Geophys. Res.*, 103, 20,487-20,500.

731   Summers, D., C. Ma, N. P. Meredith, R. B. Horne, R. M. Thorne, and R. R. Ander-

732   son (2004), Modeling outer-zone relativistic electron response to whistler-mode chorus

733   activity during substorms, *J. Atmos. Sol. Terr. Phys.*, Vol. 66, Iss. 2, pp. 133-146.

734   Thorne R. M., and C. F. Kennel (1967), Quasi-trapped VLF propagation in the outer

735   magnetosphere, *J. Geophys. Res.*, 72, 857-870.

Thorne, R.M., and R.B. Horne (1994), Landau Damping of Magnetospherically Reflected Whistlers, *Journal of Geophysical Research-Space Physics*, 99 (A9), 17249-17258.

Thorne, R. M., T. P. O'Brien, Y. Y. Shprits, D. Summers, and R. B. Horne (2005a), Timescale for MeV electron microburst loss during geomagnetic storms, *J. Geophys. Res.*, Vol. 110, A09202, doi: 10.1029/2004JA010882.

Thorne, R. M., R. B. Horne, S. A. Glauert, N. P. Meredith, Y. Y. Shprits, D, Summers, and R. R. Anderson (2005b), The influence of wave-particle interactions on relativistic electron dynamics during storms, in *Inner Magnetosphere Interactions: New Perspectives from Imaging, Geophys. Monogr. Ser.*, vol. 159, edited by James L. Burch, Michael Schulz, and Harlan Spence, pp 101-112, AGU, Washington, D. C.

Trakhtengerts, V. Yu. (1995), Magnetosphere cyclotron maser: backward wave oscillator generation regime, *J. Geophys. Res.*, Vol. 100, Iss. A9, pp. 17205-17210.

Trakhtengerts, V.Y. (1999), A generation mechanism for chorus emission, *Annales Geophysicae*, Vol. 17, pp. 95 - 100.

Tsurutani, B.T., and E.J. Smith (1974), Postmidnight chorus: A Substorm Phenomenon, *J. Geophys. Res.*, Vol. 79, No. 1, pp. 118-127.

Tsurutani, B.T., and E.J. Smith (1977), Two types of magnetospheric ELF chorus and their substorm dependences, *J. Geophys. Res.*, Vol. 82, pp. 5112-5128.

Tsyganenko, N. A., and M. I. Sitnov (2005), Modeling the dynamics of the inner magnetosphere during strong geomagnetic storms, *J. Geophys. Res.*, Vol. 110, Iss. A3, doi:10.1029/2004JA010798.

Varotsou, A., D. Boscher, S. Bourdarie, R. B. Horne, S. A. Glauert, and N. P. Meredith (2005), Simulation of the outer radiation belt electrons near geosynchronous orbit in-

759   cluding both radial diffusion and resonant interaction with whistler mode chorus waves,

760   Geophys. Res. Lett., 32, L19106, doi:10.1029/2005GL023282.

761 Walt, M. (1994), *Introduction to geomagnetically trapped radiation*, Cambridge University
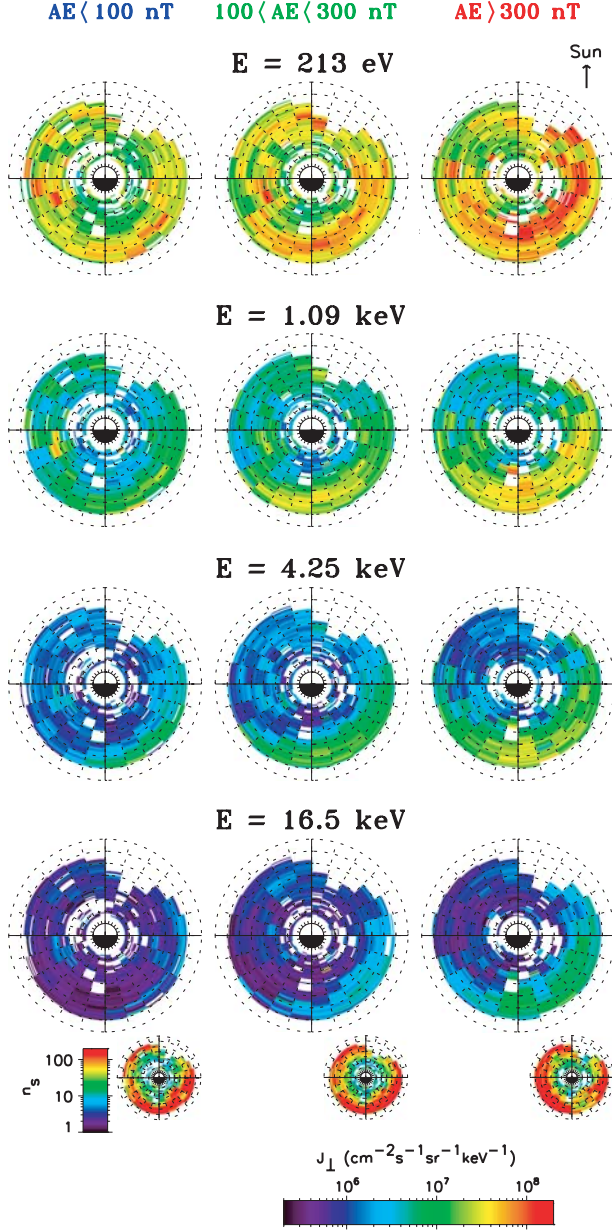
762   Press.

Figure 1.   Average suprathermal electron fluxes measured with the LEPA instrument on the CRRES satellite. Distributions are shown as a function of L-shell and MLT, parameterized by energy (rows: 0.213, 1.09, 4.25, and 16.5 keV), and magnetic activity levels (columns: AE < 100 nT, 100 < AE < 300 nT, and AE > 300 nT). The common colorbar is shown at the bottom of the figure, together with the number of samples in each L-MLT bin.
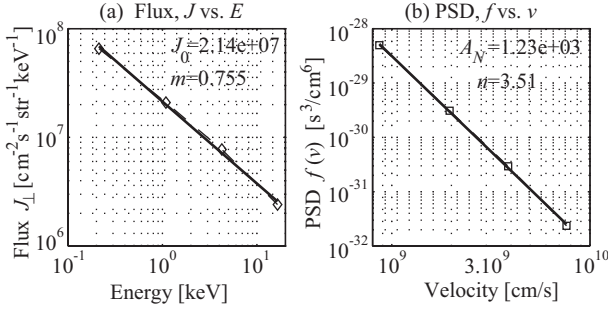
Figure 2.   Analytical fits to (a) flux values at 4 energies, and transformed into (b) phase space density (PSD) as a function of velocity, at $L = 4.45$, MLT $= 5.5$, and AE > 300 nT.
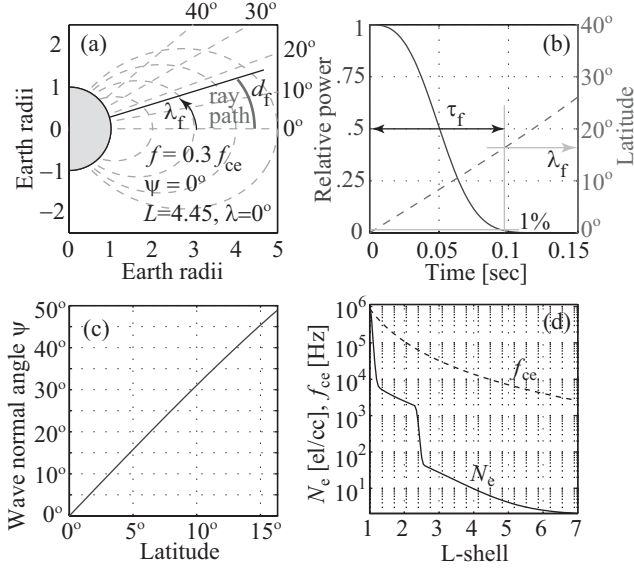
Figure 3.   Illustration of ray propagation at $L = 4.45$, MLT $= 5.5$, $\psi = 0°$, $f = 0.3 f_{\mathrm{ce}}$ and AE > 300 nT. (a) ray path shown in heavy line, with final latitude λ_f, and propagation distance d_f indicated; (b) Relative wave power (solid line) and ray latitude (dashed line) as a function of group time, showing the 1% power level which defines ray termination, giving $\tau_f = 0.0971$ sec, $\lambda_f = 16.34°$, and $d_f = 1.28 R_E$; (c) wave normal angle evolution as a function of ray latitude, and (d) equatorial electron number density used in all simulations, and electron gyrofrequency f_{ce} as a function of L-shell.
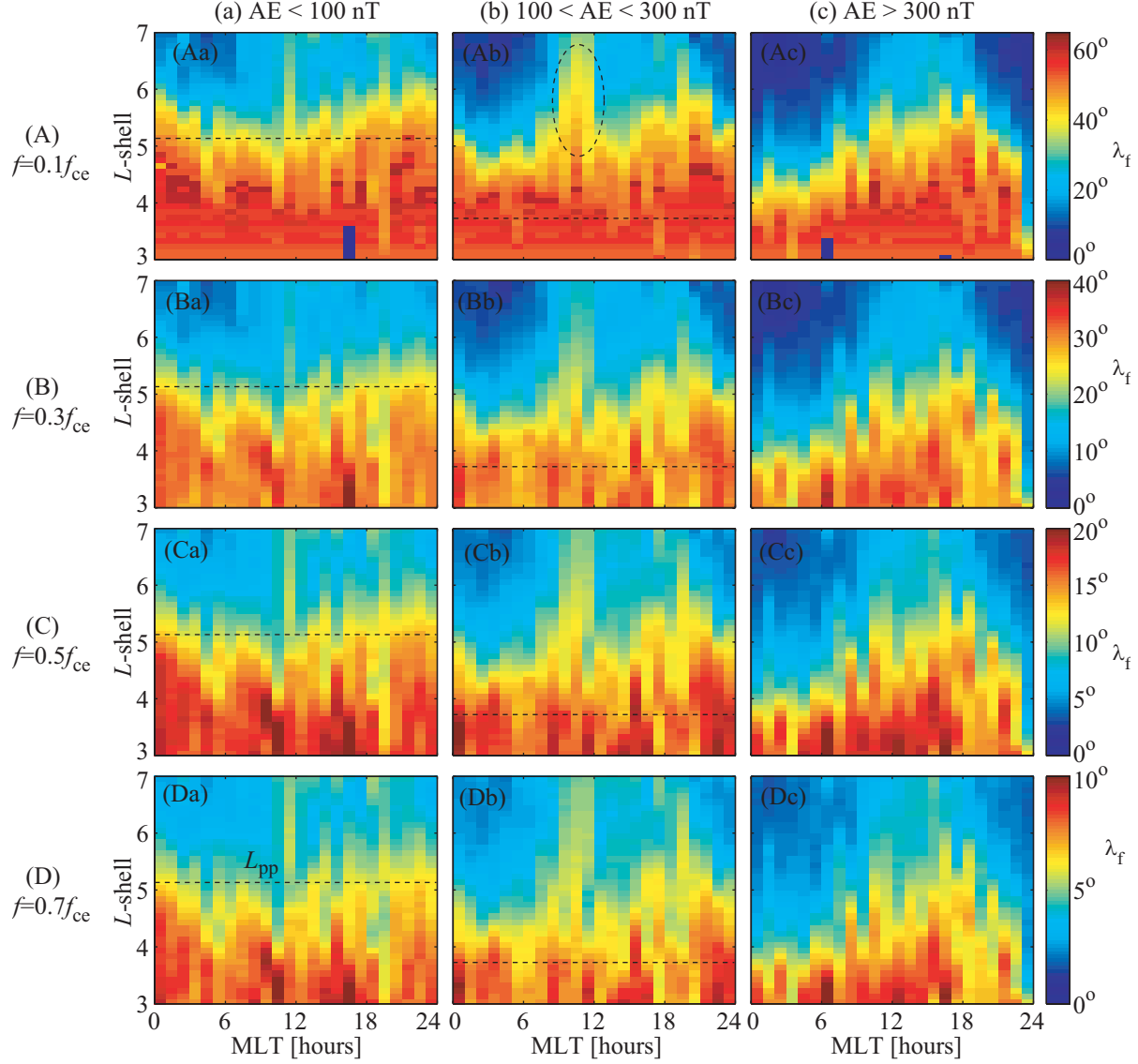
Figure 4. Final propagation latitude λ_f of rays representing chorus, shown as a function of initial L-shell (ordinate) and MLT (abscissa). Rows A–D represent the normalized frequency of each ray (f/f_{ce} = 0.1, 0.3, 0.5, and 0.7 respectively) and columns a-c represent geomagnetic activity level as indicated. Horizontal dashed lines indicate an approximate plasmapause L_{pp} location, and the oval region in panel (Ab) should be interpreted with caution since it represents a region of poor satellite coverage (c.f. Figure 1) and consists largely of interpolated flux values.
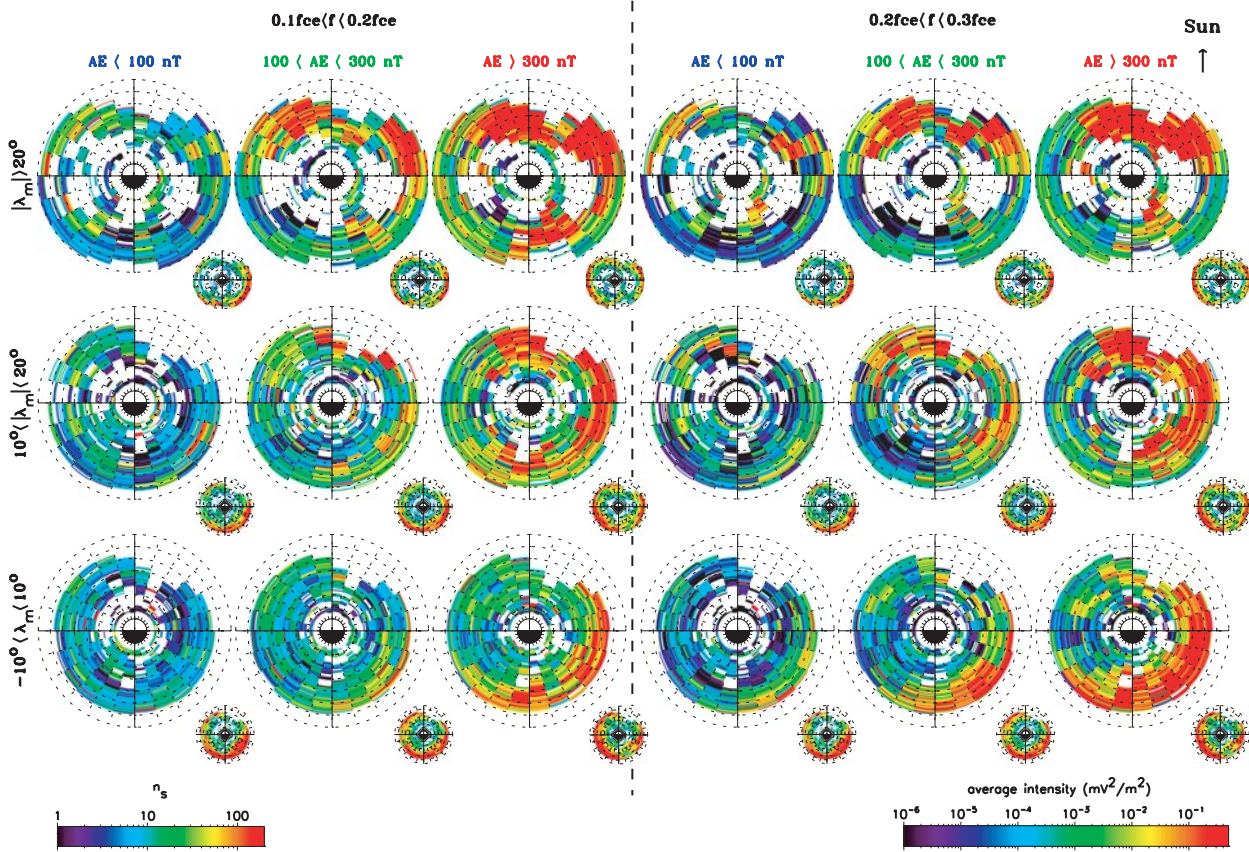
Figure 5. Distribution of chorus wave power as a function of L-shell and MLT, parameterized by magnetic latitude range, rows 1–3: $|\lambda_m| < 10°$, $10° < |\lambda_m| < 20°$, $|\lambda_m| > 20°$; and geomagnetic activity, columns 1–3: AE < 100 nT, $100 <$ AE < 300 nT, and AE > 300 nT. The 9 panels on the left and right correspond to frequency ranges of $0.1 f_{ce} < f < 0.2 f_{ce}$ and $0.2 f_{ce} < f < 0.3 f_{ce}$ respectively. The colorbars represent average wave intensity and number of samples in each bin.
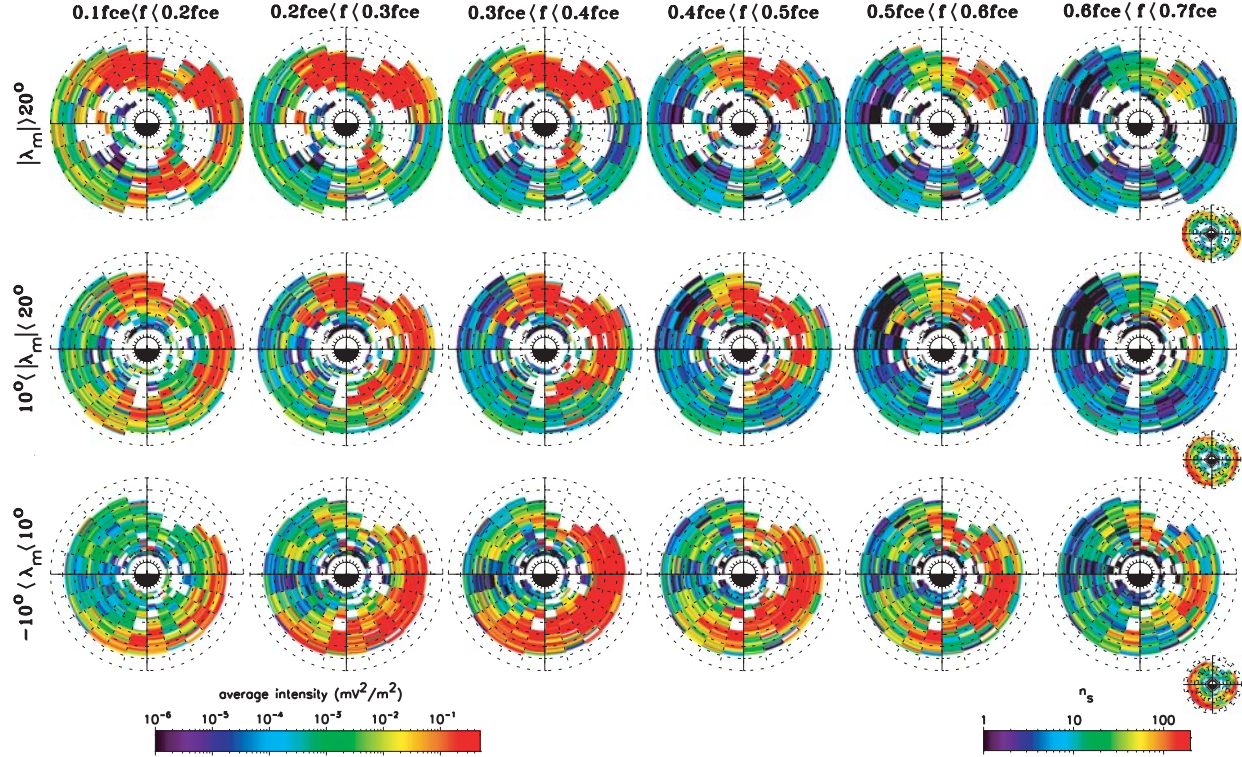
Figure 6.   Distribution of chorus wave power for active conditions (AE > 300 nT) as a function of L-shell and MLT, parameterized by magnetic latitude range, rows 1–3: $|\lambda_m| < 10°$, $10° < |\lambda_m| < 20°$, $|\lambda_m| > 20°$; and frequency band, normalized to the equatorial electron cyclotron frequency, columns 1–6: $f/f_{ce} = 0.1$–0.2, 0.2–0.3, 0.3–0.4, 0.4–0.5, 0.5–0.6, and 0.6–0.7. The colorbars represent average wave intensity and number of samples in each bin.
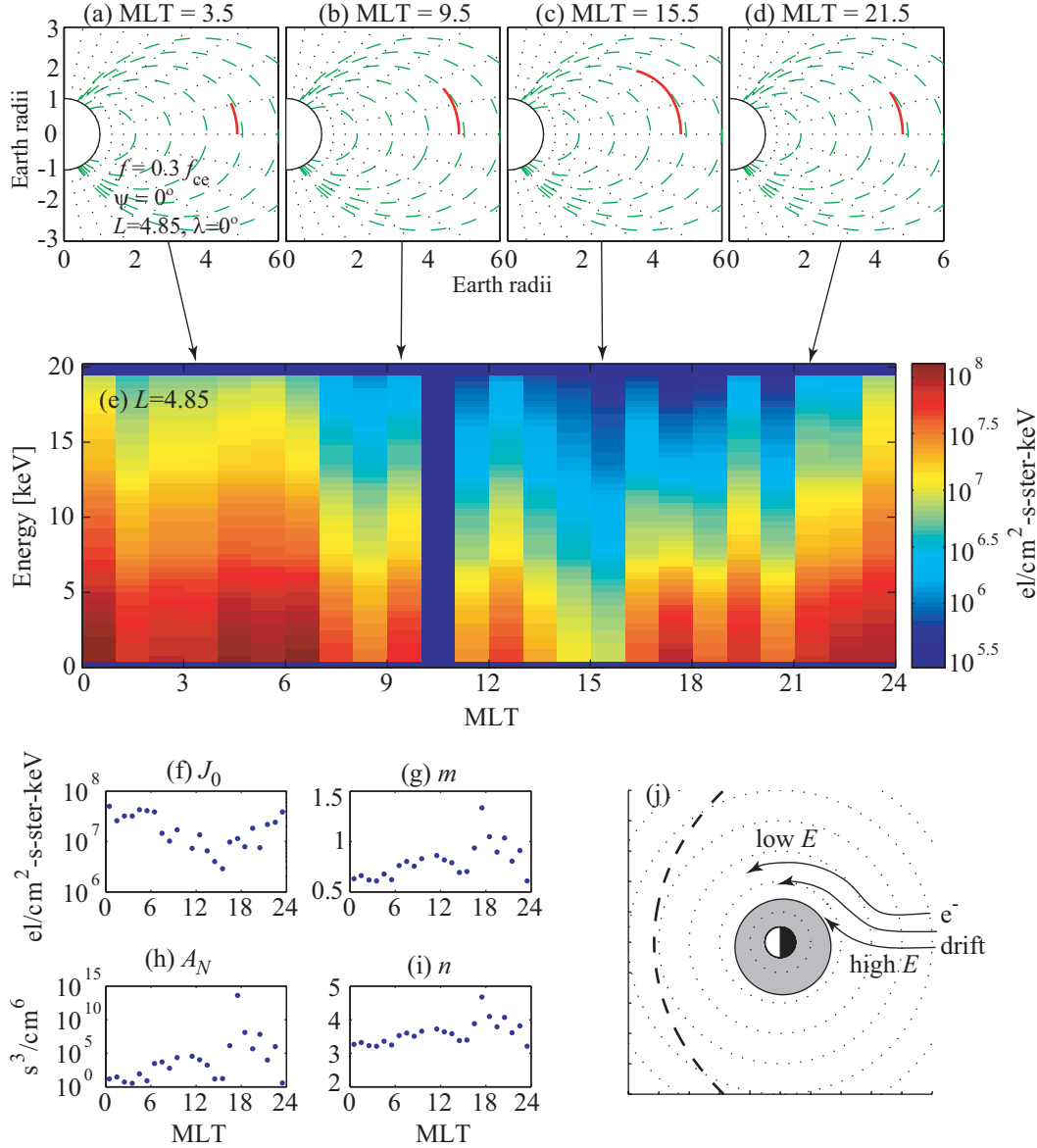
Figure 7.   Suprathermal fluxes; (a)–(d) ray paths calculated at $L = 4.85$, $f = 0.3f_{ce}$, at 4 selected MLT regions as shown; (e) suprathermal flux at $L = 4.85$ as a function of MLT and energy; (f) fitted parameters for flux distribution J_0, and (g) m; (h) fitted parameters for phase space density distribution, A_N and (i) n, all shown as a function of MLT.